

Searching for Axion-Like Particles with MAGIC and *Fermi*-LAT Data

Hai-Jun Li,^{1,2,3} Xiao-Jun Bi,^{2,3} and Peng-Fei Yin²

¹*Center for Advanced Quantum Studies, Department of Physics,
Beijing Normal University, Beijing 100875, China*

²*Key Laboratory of Particle Astrophysics, Institute of High Energy Physics,
Chinese Academy of Sciences, Beijing 100049, China*

³*School of Physics, University of Chinese Academy of Sciences, Beijing 100049, China*

(Dated: March 17, 2022)

In this work, we reanalyze the axion-like particle (ALP)-photon oscillation effect in the γ -ray spectra of the blazars Markarian 421 (Mrk 421) and PG 1553+113 using the Major Atmospheric Gamma Imaging Cherenkov Telescopes (MAGIC) and *Fermi* Large Area Telescope (*Fermi*-LAT) data. These data are collected during the common operation time, which cover twenty activity phases of these blazars. Not all the observations of these phases can be individually used to set the 95% confidence level (C.L.) constraint on the ALP parameter space. However, the constraint can be significantly improved if the analyses for the observations of these phases are combined. We release the combined constraints results of the sources Mrk 421 with fifteen phases and PG 1553+113 with five phases, respectively. For Mrk 421, we find that the γ -ray observations of MAGIC and *Fermi*-LAT have excluded the ALP parameter region with the ALP-photon coupling of $g_{a\gamma} \gtrsim 2 \times 10^{-11} \text{ GeV}^{-1}$ for the ALP mass of $\sim 8 \times 10^{-9} \text{ eV} \lesssim m_a \lesssim 2 \times 10^{-7} \text{ eV}$ at 95% C.L. However, we find that the ALP-photon oscillation would improve the fit to the observed spectra of PG 1553+113 and find some favored parameter regions at 95% C.L.

I. INTRODUCTION

The strong Charge-Parity (CP) problem [1–3] is the long standing puzzle in the Standard Model (SM) of particle physics as the tiny value of

$$\bar{\theta} < 10^{-10} \ll 1. \quad (1)$$

The quantum chromodynamics (QCD) axion [4, 5] can be described as the pseudo Nambu-Goldstone boson of a spontaneously broken $U(1)_{\text{PQ}}$ symmetry, also called PQ symmetry [6, 7], would solve the strong- CP problem [8–10]. Two QCD axion benchmark models are currently quite popular in the literature, the Kim-Shifman-Vainshtein-Zakharov (KSVZ) [11, 12] and Dine-Fischler-Srednicki-Zhitnitsky (DFSZ) [13, 14] models. Apart from the canonical QCD axion, various axion-like particles (ALPs) have also been proposed in the new physics model beyond the SM, such as string models [15–17]. If ALPs are produced nonthermally in the early Universe, they could also be candidates of the dark matter (DM) [18–22].

The ALP mass m_a and the coupling constant with photons $g_{a\gamma}$ are taken to be two independent parameters in the research [5]. This is different from the scenario of the QCD axion, where these two parameters are related to each other. The coupling between the ALP and photons would lead to ALP-photon oscillation for the photons ejecting from the high energy γ -ray sources which are far from the Earth and would modify their γ -ray energy spectra [23]. This effect could lead to observable modifications in the γ -ray telescopes [24, 25]. Many works have been performed to study this effect for many astrophysical sources and set constraints on the ALP parameter space [24–59].

In our previous work [51], we investigate the ALP-

photon oscillation effect in the high energy γ -ray spectra of the sources PKS 2155–304 and PG 1553+113 measured by H.E.S.S. and *Fermi* Large Area Telescope (*Fermi*-LAT) [60]. These data are collected during the common operation time. We find that the ALP-photon oscillation would improve the fit to the observed spectra of PKS 2155–304 and PG 1553+113 and find a favored parameter region at 95% confidence level (C.L.). In Ref. [52], we investigate the ALP-photon oscillation effect in the spectra of the blazar Markarian 421 (Mrk 421) using 4.5-year of the Astrophysical Radiation with Ground-based Observatory at YangBaJing (ARGO-YBJ) and *Fermi*-LAT data with then phases [61]. We also combine the results of all the phases together to set constraint on the ALP parameter space. The constraint can be significantly improved if the analyses for the ten phases are combined.

In this work, we reanalyze the effect of the ALP-photon oscillation in the high energy γ -ray spectra of the sources Mrk 421 and PG 1553+113. We focus on the very high energy (VHE) γ -ray observations of these two blazars with the Major Atmospheric Gamma Imaging Cherenkov Telescopes (MAGIC) data in Ref. [62]. Additionally, the lower energy (from 0.1 to 100 GeV) spectra data of Mrk 421 and PG 1553+113 are taken by the *Fermi*-LAT during the similar time ranges as the MAGIC observations. We also combine the results of the sources Mrk 421 with fifteen phases and PG 1553+113 with five phases together to set constraint on the ALP parameter space.

This paper is organized as follows. Sec. II is the ALP-photon oscillation. In Sec. III, we introduce the propagation of high energy γ -ray with the ALP-photon oscillation in three parts, including the source region, the extragalactic space, and the Milky Way region. In Sec. IV, we introduce the data fitting and statistical methods. In

Sec. V, we give the constraints on the ALP parameter space from the γ -ray observations. The combined constraints results of the sources Mrk 421 and PG 1553+113 on the ALP parameter space are also given. The conclusion is given in Sec. VI.

II. ALP-PHOTON OSCILLATION

The ALP-photon oscillation effect occurring in the magnetic field would modify the γ -ray energy spectra of astrophysical sources, which are far from the Earth [24, 25]. The effective Lagrangian for the ALP-photon coupling can be described by [23]

$$\mathcal{L}_{\text{ALP}} = \frac{1}{2}\partial^\mu a \partial_\mu a - \frac{1}{2}m_a^2 a^2 - \frac{1}{4}g_{a\gamma} a F_{\mu\nu} \tilde{F}^{\mu\nu}, \quad (2)$$

where a is the ALP field, m_a is the ALP mass, $g_{a\gamma}$ is the coupling constant, $F_{\mu\nu}$ and $\tilde{F}^{\mu\nu}$ are the electromagnetic field tensor and the dual tensor, respectively.

The ALP and photon are interconvertible in the external magnetic field and could be described by the ALP-photon beam [29]

$$\Psi = (A_1, A_2, a)^T, \quad (3)$$

where A_1 and A_2 represent the photon transverse polarization states in the directions of x_1 and x_2 which are perpendicular to the propagation direction x_3 , respectively.

The density matrix of the ALP-photon system is given by

$$\rho = \Psi \otimes \Psi^\dagger, \quad (4)$$

that obeys the Liouville-Von Neumann (LVN) equation [27]

$$i \frac{d\rho(s)}{ds} = [\rho, \mathcal{M}_0]. \quad (5)$$

Assuming that B_T is the transversal magnetic field aligned along x_2 , the mixing matrix \mathcal{M}_0 is

$$\mathcal{M}_0 = \begin{pmatrix} \Delta_{\text{pl}} & 0 & 0 \\ 0 & \Delta_{\text{pl}} & \Delta_{a\gamma} \\ 0 & \Delta_{a\gamma} & \Delta_{aa} \end{pmatrix}, \quad (6)$$

with

$$\Delta_{\text{pl}} = -\frac{\omega_{\text{pl}}^2}{2E} \simeq -1.1 \times 10^{-4} \text{ kpc}^{-1} n_{\text{cm}^{-3}} E_{\text{GeV}}^{-1}, \quad (7)$$

$$\Delta_{a\gamma} = \frac{1}{2} g_{a\gamma} B_T \simeq 1.52 \times 10^{-2} \text{ kpc}^{-1} g_{11} B_{\mu\text{G}}, \quad (8)$$

$$\Delta_{aa} = -\frac{m_a^2}{2E} \simeq -7.8 \times 10^{-2} \text{ kpc}^{-1} m_{\text{neV}}^2 E_{\text{GeV}}^{-1}, \quad (9)$$

where $\omega_{\text{pl}} \sim \sqrt{4\pi\alpha n_e/m_e}$ is the plasma frequency, α is the fine-structure constant, and n_e is the number density of free electron. In the above equations, we have used the notations $n_{\text{cm}^{-3}} \equiv n_e/1 \text{ cm}^{-3}$, $E_{\text{GeV}} \equiv E/1 \text{ GeV}$,

$g_{11} \equiv g_{a\gamma}/10^{-11} \text{ GeV}^{-1}$, $B_{\mu\text{G}} \equiv B_T/1 \mu\text{G}$, and $m_{\text{neV}} \equiv m_a/1 \text{ neV}$.

For a general magnetic field form an angle ψ with x_2 , the mixing matrix \mathcal{M}_0 becomes

$$\mathcal{M} = V(\psi) \mathcal{M}_0 V^\dagger(\psi), \quad (10)$$

with

$$V(\psi) = \begin{pmatrix} \cos \psi & \sin \psi & 0 \\ -\sin \psi & \cos \psi & 0 \\ 0 & 0 & 1 \end{pmatrix}. \quad (11)$$

After oscillation in numerous consecutive domains, the final density matrix of the ALP-photon system is

$$\rho(s) = T(s) \rho(0) T^\dagger(s), \quad (12)$$

where $T(s)$ is the whole transfer matrix for the propagation distance s

$$T(s) = \prod_i^n \mathcal{M}(i). \quad (13)$$

$\mathcal{M}(i)$ is the mixing matrix in the i -th region. The initial beam state $\rho(0)$ is assumed to be

$$\rho(0) = \frac{1}{2} \text{diag}(1, 1, 0). \quad (14)$$

The final survival probability of the photon in the ALP-photon system is given by [29]

$$P_{\gamma\gamma} = \text{Tr}((\rho_{11} + \rho_{22}) T(s) \rho(0) T^\dagger(s)), \quad (15)$$

with

$$\rho(s)_{11} = \text{diag}(1, 0, 0), \quad \rho(s)_{22} = \text{diag}(0, 1, 0). \quad (16)$$

The ALP-photon conversion would become maximal and energy-independent in the strong mixing regime $E_{\text{crit}} \lesssim E \lesssim E_{\text{max}}$ with [35, 41]

$$E_{\text{crit}} = \frac{|m_a^2 - \omega_{\text{pl}}^2|}{2g_{a\gamma} B_T} \simeq 2.5 \text{ GeV} |m_{\text{neV}}^2 - 1.4 \times 10^{-3} n_{\text{cm}^{-3}}| g_{11}^{-1} B_{\mu\text{G}}^{-1}, \quad (17)$$

and

$$E_{\text{max}} = \frac{90\pi}{7\alpha} \frac{B_{\text{cr}}^2 g_{a\gamma}}{B_T} \simeq 2.12 \times 10^6 \text{ GeV} g_{11} B_{\mu\text{G}}^{-1}, \quad (18)$$

where $B_{\text{cr}} = m_e^2/|e| \sim 4.41 \times 10^{13} \text{ G}$ is the critical magnetic field.

III. ALP-PHOTON PROPAGATION

In order to obtain the transfer matrix for the ALP-photon system, the propagation process of the system is divided into three parts, including the propagations in the source region, the extragalactic space, and the Milky Way region [25, 35].

We neglect the internal γ -ray absorption and the ALP-photon oscillation within the broad line region of the source, and consider the ALP-photon oscillation effect in the blazar jet magnetic field (BJMF). Following Refs. [43, 52, 63], here the BJMF of Mrk 421 and PG 1553+113 are considered as the BL Lac type with the transverse magnetic field $B_{\text{jet}}(r)$ and the electron density $n_{\text{el}}(r)$ profiles. The radial profile of the magnetic field strength is [64–66]

$$B_{\text{jet}}(r) = B_0 \left(\frac{r}{r_{\text{VHE}}} \right)^{-1}, \quad (19)$$

where r_{VHE} is the distance of the VHE emission site to the central black hole and B_0 is the core magnetic field strength at r_{VHE} . The modified model for the electron density distribution is [67]

$$n_{\text{el}}(r) = n_0 \left(\frac{r}{r_{\text{VHE}}} \right)^{-2}, \quad (20)$$

where n_0 is the electron density at r_{VHE} . r_{VHE} is given by $r_{\text{VHE}} \sim R_{\text{VHE}}/\theta_{\text{jet}}$, where R_{VHE} is the radius of the VHE emitting plasma blob and θ_{jet} is the angle between the jet axis and the line of sight. Above equations hold in the co-moving frame of the blazar jet. The photon energy E_j in this frame is related to the energy E_L in the laboratory frame with the transformation $E_j = E_L/\delta_D$, where δ_D is the Doppler factor. In the region with $r > 1$ kpc, the BJMF is set to be zero. More details about this BJMF model can be found in Refs. [43, 63].

In principle, the parameters of the BJMF model can be derived from the fit to the data using the synchrotron self-Compton model. It is difficult to derive the precise value of r_{VHE} from the observations. In Ref. [52], we find $r_{\text{VHE}} \sim \mathcal{O}(10^{17}) - \mathcal{O}(10^{18})$ cm in Mrk 421. Following Refs. [52, 68], for Mrk 421 and PG 1553+113, we set $r_{\text{VHE}} = 1 \times 10^{17}$ cm, $\delta_D = 30$, and $n_0 = 3 \times 10^3 \text{ cm}^{-3}$ as the benchmark parameters for all the phases. In Ref. [68], the parameter B_0 of Mrk 421 and PG 1553+113 are set to be 0.09 G and 1.1 G, respectively. We shall take $B_0 = 0.1$ G and 1.0 G for Mrk 421 and PG 1553+113 as the benchmark parameters for all the phases, respectively.

Beyond R_{VHE} , ALP-photon system propagates outwards unimpeded until it leave the jet and enter the host galaxy. Following Refs. [43, 69], we do not consider the ALP-photon oscillation effect in the magnetic field of the host galaxy since it is too small. The blazar may be located at a rich cluster, where the turbulent inter-cluster magnetic field (ICMF) is about $\mathcal{O}(1) \mu\text{G}$ [70–72]. We find that the ALP-photon oscillation could be significant in this magnetic field [35]. However, there is no evidence that Mrk 421 and PG 1553+113 are reside in such a rich environment. Therefore, we do not consider the ALP-photon oscillation effect in the ICMF ¹.

The upper limit of the extragalactic magnetic field on the largest cosmological scale is $\mathcal{O}(1)$ nG [73]. Its actual value is not clear and would be much lower than this upper limit [44, 74]. Following Ref. [52], we do not consider the effect of the extragalactic magnetic field for the ALP-photon system propagation in the extragalactic space and only focus on the attenuation effect induced by the extragalactic background light (EBL) due to the pair production process $\gamma + \gamma_{\text{BG}} \rightarrow e^+ + e^-$. This attenuation effect can be characterized by the factor of $e^{-\tau}$ with the optical depth [28, 75]

$$\tau = c \int_0^{z_0} \frac{dz}{(1+z)H(z)} \int_{E_{\text{th}}}^{\infty} d\omega \frac{dn(z)}{d\omega} \bar{\sigma}(E_\gamma, \omega, z), \quad (21)$$

where z_0 is the redshift of the source, $H(z)$ is the rate of the Hubble expansion, E_{th} is the threshold energy, $\bar{\sigma}$ is the integral cross section of the pair production, E_γ and ω are the source and background photon energies, respectively, and $dn/d\omega$ is the proper number density of the EBL. The EBL model used here is taken from Ref. [75]. The redshift of Mrk 421 and PG 1553+113 are taken as $z_0 = 0.031$ and 0.45, respectively.

For the propagation of the ALP-photon system in the Milky Way region, we consider the ALP-photon oscillation effect in the galactic magnetic field (GMF). Here we neglect the random component on the small scale and take the regular component of the GMF on the large scale from Ref. [76].

IV. GAMMA-RAY DATA FITTING AND STATISTICAL METHODS

The MAGIC [77, 78] is a system of two imaging atmospheric Cherenkov telescopes (IACTs) located at the Roque de los Muchachos Observatory in Spain. The telescopes record images of extensive air showers in stereoscopic mode, enabling the observations of VHE gamma-ray sources at energies $\gtrsim 50$ GeV [62]. Their data analysis is performed using the standard MAGIC analysis and reconstruction software MARS [78]. All data used in this work were taken during dark nights in good weather conditions.

The *Fermi*-LAT [79] is an imaging, wide field-of-view, high-energy γ -ray telescope, covering the energy range from below 20 MeV to more than 300 GeV. The detector is fully covered by a segmented anticoincidence shield that provides a highly efficient vetoing against charged particle background events. The *Fermi*-LAT data are extracted from the data files available at the FSSC data center ².

¹ In Ref. [35], they consider the effect of BJMF and ICMF of PG 1553+113 on ALP-photon oscillation separately. In Ref. [51], we just consider the ICMF effect of PG 1553+113 and find that the constraint result on the ALP parameter space is more weaker than that of H.E.S.S. [48] and *Fermi*-LAT [49]. So we neglect the ICMF effect of PG 1553+113 in this work.

² <https://fermi.gsfc.nasa.gov/ssc/data/access/>

¹ In Ref. [35], they consider the effect of BJMF and ICMF of PG

In Ref. [62], the MAGIC collaboration reported the spectral variations of Mrk 421 and PG 1553+113 at different wavebands and divided the whole observation periods into fifteen phases and five phases, respectively. The γ -ray spectra of Mrk 421 and PG 1553+113 at lower energies in the common operation time from *Fermi*-LAT are also analysed in Ref. [62]. The analysis is performed with the standard ScienceTool³ and the corresponding threads provided by *Fermi*-LAT.

In order to fit the experimental data from MAGIC and *Fermi*-LAT under the null hypothesis, the models of the intrinsic energy spectra of the blazars Mrk 421 and PG 1553+113 are taken as Ref. [62]. The intrinsic blazar energy spectra $\Phi_{\text{int}}(E)$ can be described by simple and smooth concave functions with three to five parameters: Power Law with Exponential cut-off (EPWL), Power Law with SuperExponential cut-off (SEPWL), Log Parabola (LP), and Log Parabola with Exponential cut-off (ELP). The functional expressions for these differential spectra, dF/dE , are the following:

- EPWL:

$$\Phi_{\text{int}}(E) = F_0 \left(\frac{E}{E_0}\right)^{-\Gamma} \exp\left(-\frac{E}{E_c}\right), \quad (22)$$

- SEPWL:

$$\Phi_{\text{int}}(E) = F_0 \left(\frac{E}{E_0}\right)^{-\Gamma} \exp\left(-\left(\frac{E}{E_c}\right)^d\right), \quad (23)$$

- LP:

$$\Phi_{\text{int}}(E) = F_0 \left(\frac{E}{E_0}\right)^{-\Gamma - b \log\left(\frac{E}{E_0}\right)}, \quad (24)$$

- ELP:

$$\Phi_{\text{int}}(E) = F_0 \left(\frac{E}{E_0}\right)^{-\Gamma - b \log\left(\frac{E}{E_0}\right)} \exp\left(-\frac{E}{E_c}\right), \quad (25)$$

where F_0 , Γ , E_c , b , and d are treated as free parameters, for EPWL and SEPWL, E_0 is taken to be 1 GeV, while for LP and ELP, E_0 is a free parameter. For a single phase, we choose the intrinsic energy spectrum with the minimum best-fit reduced χ^2 under the null hypothesis. However, we just consider one intrinsic energy spectrum model with ten phases of the Mrk 421 observations in Ref. [52]. The intrinsic energy spectra models of the twenty phases of Mrk 421 and PG 1553+113 in this work are listed in Table I.

Considering the modification of the energy spectrum induced by the ALP, the expected γ -ray energy spectrum

under the ALP hypothesis is determined by the survival probability of the photon $P_{\gamma\gamma}$ in Eq. (15) [52]

$$\Phi_{\text{w ALP}}(E) = P_{\gamma\gamma} \Phi_{\text{int}}(E), \quad (26)$$

with the intrinsic energy spectrum $\Phi_{\text{int}}(E)$. We also take into account the energy dispersion function and the energy resolution of the experiment in the analysis. The energy resolution of MAGIC is adopted to be 16% [78]. Considering the energy dispersion function $D(E', E_1, E_2)$ where E' is the actual energy, the expected γ -ray flux at the detector in the energy bin between E_1 and E_2 can be derived as [51]

$$\Phi' = \frac{\int_0^\infty D(E', E_1, E_2) \Phi(E') dE'}{E_2 - E_1}, \quad (27)$$

where $\Phi(E')$ is the γ -ray spectrum before detection. The χ^2 value is given by [62]

$$\chi^2 = \left(\frac{\Phi'(E_{\text{LAT}}) - F_{\text{LAT}}}{\Delta F_{\text{LAT}}}\right)^2 + \left(\frac{\Gamma_{\text{fit}} - \Gamma_{\text{LAT}}}{\Delta \Gamma_{\text{LAT}}}\right)^2 + \sum_{i=1}^N \left(\frac{\Phi'(E_i) - \tilde{\phi}_i}{\delta_i}\right)^2, \quad (28)$$

where E_{LAT} , F_{LAT} , Γ_{LAT} , and Γ_{fit} are the central energy of the energy bin bow, the observed energy flux, the local energy spectrum index, and the fitted local expected energy spectrum index of *Fermi*-LAT, respectively. N is the point number of MAGIC, $\Phi'(E_i)$ is the expected γ -ray flux, $\tilde{\phi}_i$ is the observed flux, and δ_i is the corresponding uncertainty of the observation.

In order to set the constraint on the ALP parameter space, we define the threshold value χ_{th}^2 as

$$\chi_{\text{th}}^2 = \chi_{\text{min}}^2 + \Delta\chi^2, \quad (29)$$

with the minimum best-fit χ_{min}^2 in the $m_a - g_{a\gamma}$ plane and the $\Delta\chi^2$ corresponding to the particular confidence level. Due to the non-linear dependence of the spectral irregularities on the ALP parameters and possible systematics in the observations, we derive the value of $\Delta\chi^2$ from the Monte Carlo simulation [49].

Following Ref. [52], we generate 400 sets of the observed γ -ray spectra of Mrk 421 and PG 1553+113 in the pseudo-experiments that are realized by Gaussian samplings [45]. For each set of the simulated spectrum, we can derive the best-fit χ^2 for both the null hypothesis $\hat{\chi}_{\text{null}}^2$ and the ALP hypothesis $\hat{\chi}_{\text{w ALP}}^2$. For each Monte Carlo data set, we have the test statistic (TS) value

$$\text{TS} = \hat{\chi}_{\text{null}}^2 - \hat{\chi}_{\text{w ALP}}^2. \quad (30)$$

Then we obtain the TS distribution under the null hypothesis for all data sets that obeys the non-central χ^2 distribution. The $\Delta\chi^2$ corresponding to the certain confidence level can be derived from the TS distribution with the effective degree of freedom (d.o.f.) and the non-centrality λ . Finally, we assume that the probability distribution under the alternative hypothesis with ALP is approximated with the distribution under the null hypothesis and use the value of $\Delta\chi^2$ derived above to set the constraint on the ALP parameter space [49].

³ <https://fermi.gsfc.nasa.gov/ssc/data/analysis/scitools>

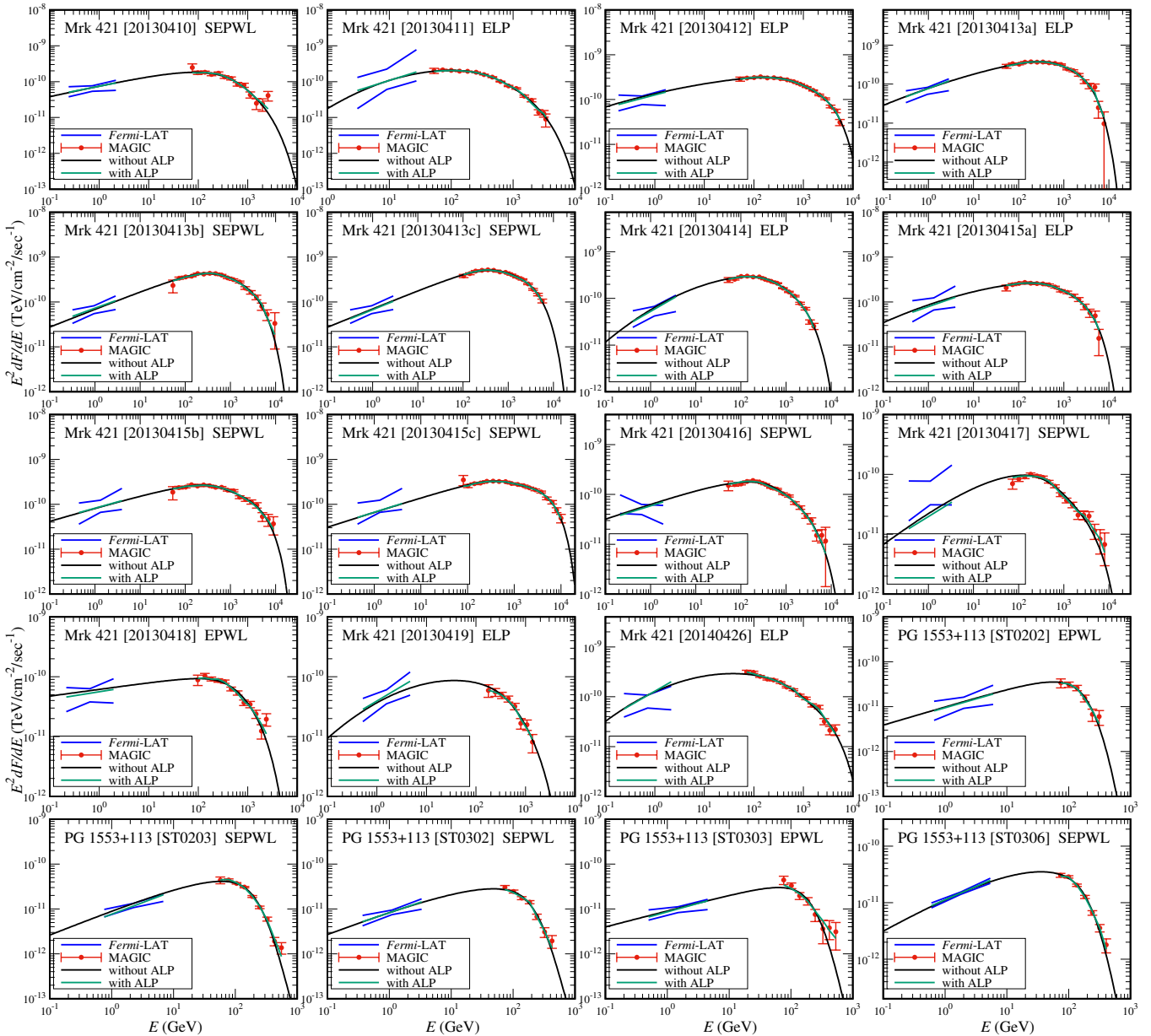


FIG. 1. The best-fit γ -ray spectra of Mrk 421 and PG 1553+113 with fifteen phases and five phases, respectively. The black lines represent the spectra under the null hypothesis. The green lines represent the spectra under the ALP hypothesis with minimum best-fit χ^2_{\min} in the $m_a - g_{a\gamma}$ plane. The values of the χ^2 are given by Table I. The experimental data are from MAGIC and *Fermi*-LAT [62].

V. CONSTRAINTS ON ALP PARAMETER SPACE

In this section, we set constraints on the ALP parameter space using the data of MAGIC and *Fermi*-LAT in the twenty phases of Mrk 421 and PG 1553+113. The best-fit values of $\chi^2_{w/oALP}$ under the null hypothesis are listed in Table I. In Fig. 1, we also give the best-fit γ -ray spectra for the twenty phases under the null and ALP hypotheses. We can see that the null hypothesis can well fit the MAGIC and *Fermi*-LAT data. The distributions of

χ^2_{wALP} under the ALP hypothesis in the twenty phases are shown in Fig. 2 with the benchmark values of the BJMF parameters. The green lines in Fig. 1 represent the spectra under the ALP hypothesis with minimum best-fit χ^2_{\min} in the $m_a - g_{a\gamma}$ plane.

We can derive the TS distributions for the twenty phases of Mrk 421 and PG 1553+113. We find that the non-centralities of all the TS distributions are about 0.01. The effective d.o.f. of the distributions and the threshold values of $\Delta\chi^2$ corresponding to 95% C.L. are listed in Table I. Then we can derive the values of $\Delta\chi^2$ corre-

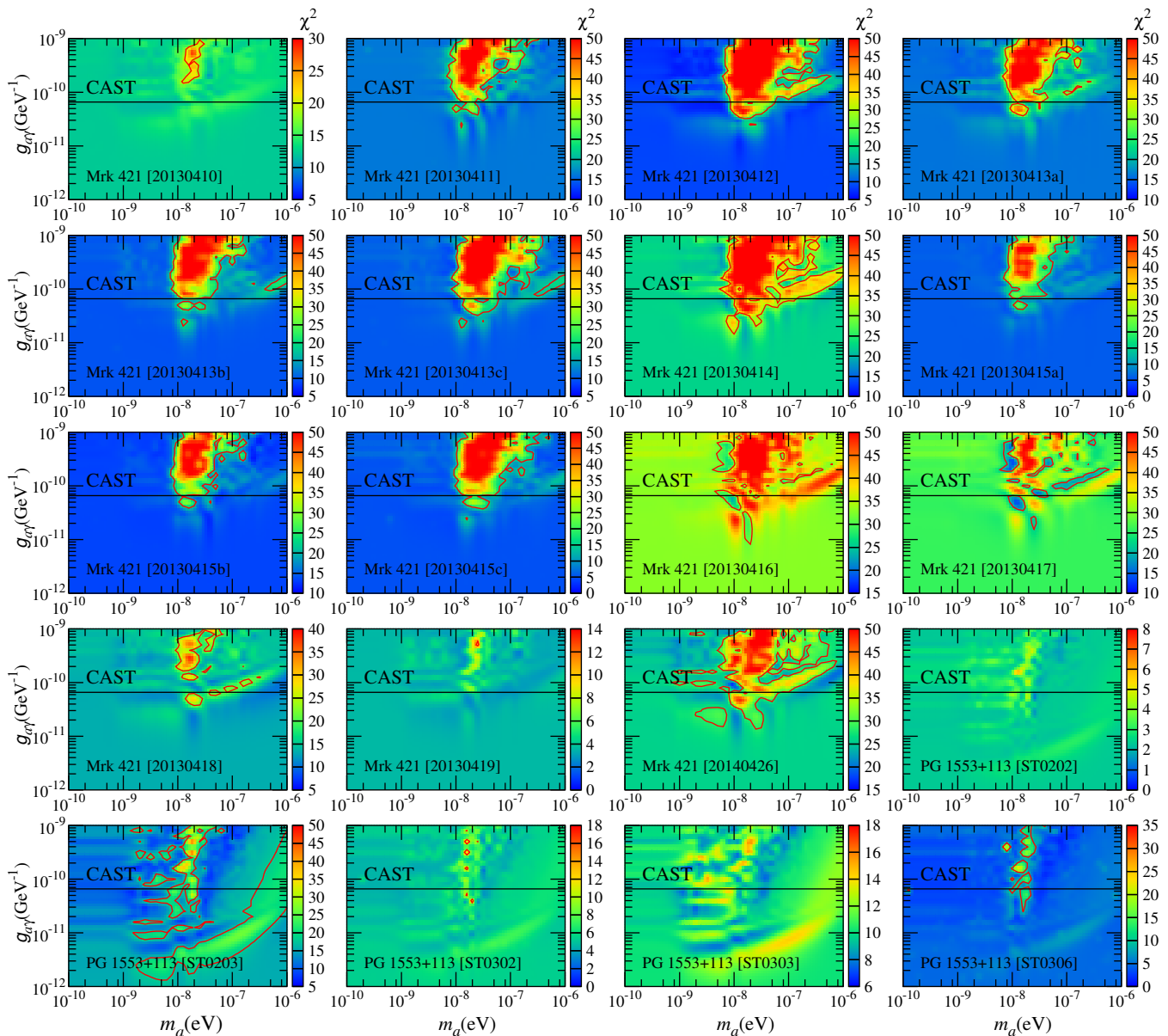


FIG. 2. The distributions of χ_w^2 in the $m_a - g_{a\gamma}$ plane for the fifteen phases of Mrk 421 and five phases of PG 1553+113, respectively. The red contours represent the excluded regions at 95% C.L. The horizontal line represents the upper bound on $g_{a\gamma}$ set by CAST [80] of $g_{a\gamma} < 6.6 \times 10^{-11}$ GeV $^{-1}$.

sponding to the 95% C.L. threshold as shown in Table I. With the values of $\Delta\chi^2$ for all the phases, the constraints on the ALP parameter space at 95% C.L. from Mrk 421 and PG 1553+113 are shown in Fig. 2. The red contours in Fig. 2 represent the upper limits at 95% C.L. We find that not all the observations of these phases can be individually used to set the 95% C.L. constraint on the ALP parameter space.

Following Ref. [52], in order to make a reliable implication, we combined the constraints results together for the fifteen phases of Mrk 421 and the five phases of PG 1553+113, respectively. The BJMF configurations during all the phases of Mrk 421 and PG 1553+113 are

assumed to be steady⁴. The combined χ_w^2 distributions in the $m_a - g_{a\gamma}$ plane and the χ^2 data of Mrk 421 and PG 1553+113 are shown in Fig. 3 and Table I, respectively. The red contours in Fig. 3 represent the combined upper limits at 95% C.L.

⁴ In Ref. [52], the BJMF configurations of the ten phases (lasted about 4.5 years) of Mrk 421 by ARGO-YBJ and *Fermi*-LAT can be found in Ref. [61]. However, the BJMF parameters of Mrk 421 and PG 1553+113 used in this work are not given in Ref. [62]. Since the phases durations are relatively short here, we can assume that the BJMF configurations are steady.

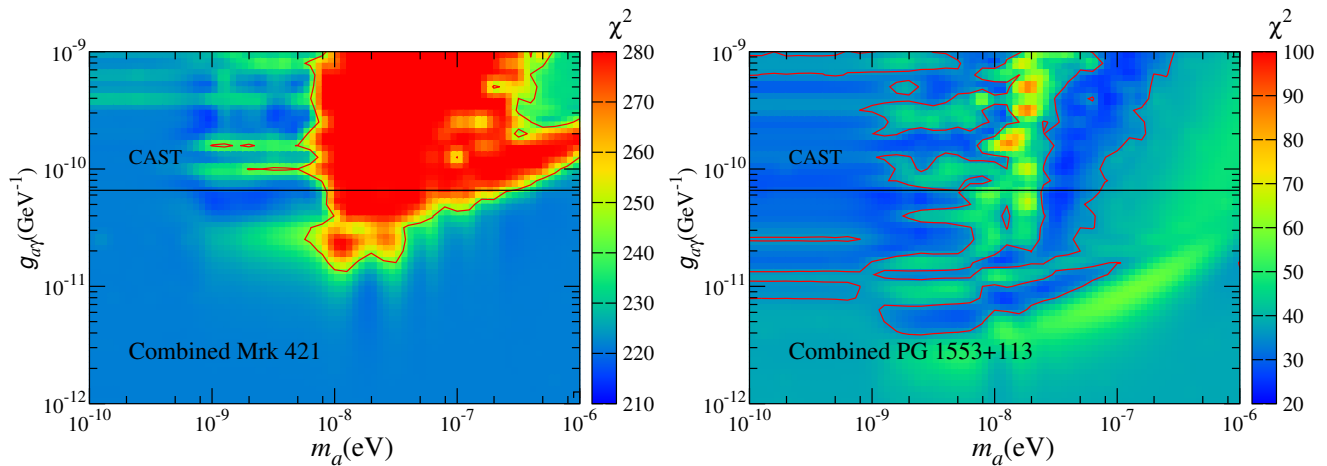


FIG. 3. The distributions of χ^2_{wALP} in the $m_a - g_{a\gamma}$ plane for the combined phases of Mrk 421 (Left) and PG 1553+113 (Right). The red contours represent the excluded regions at 95% C.L.

For comparison, we also show the constraints results on the ALP parameter space from the PKS 2155–304 observation of H.E.S.S. [48], the NGC 1275 observation of *Fermi*-LAT [49], the Mrk 421 observations of ARGO-YBJ and *Fermi*-LAT [52], and the PG 1553+113 observations of H.E.S.S. II and *Fermi*-LAT [51] in Fig. 4.

Mrk 421—The best-fit reduced χ^2 under the null hypothesis in the fifteen phases are around the average value 1.10. We notice that the results of these phases are very different from the results of other phases, such as the phases Mrk 421 [20130416] and Mrk 421 [20130417], we find that the data in these phases favor the ALP hypothesis. This also can be seen from the small values of χ^2_{\min} and χ^2_{th} under the ALP hypothesis for these phases shown in Table I. Compared with the limit set by CAST [80] about $g_{a\gamma} < 6.6 \times 10^{-11}$ GeV $^{-1}$, the combined limit set by the Mrk 421 observations of MAGIC and *Fermi*-LAT excludes the ALP parameter region with the ALP-photon coupling of $g_{a\gamma} \gtrsim 2 \times 10^{-11}$ GeV $^{-1}$ for the ALP mass of $\sim 8 \times 10^{-9}$ eV $\lesssim m_a \lesssim 2 \times 10^{-7}$ eV at 95% C.L. This combined constraint result is not coincide completely with that derived from the observations data of ARGO-YBJ and *Fermi*-LAT in Ref. [52].

PG 1553+113—The best-fit reduced χ^2 under the null hypothesis in the five phases are around the average value 1.23. It can be seen that the data sets of these five phases set very different constraints. Only using the data of the phases PG 1553+113 [ST0203] and PG 1553+113 [ST0306], we could find some excluded ALP parameter regions at 95% C.L. The constraint result of the phase PG 1553+113 [ST0203] is also stricter than that derived from the observations data of PG 1553+113 in Ref. [51]. For the other phases, we could not set the 95% C.L. constraint in the $m_a - g_{a\gamma}$ plane. This is because that the observations in these phases provide too few data points. For the combined result, we find that the ALP-photon oscillation would improve the fit to the PG 1553+113 observations of MAGIC and *Fermi*-LAT and find some

favorable parameter regions at 95% C.L.

Finally, we discuss the impact of the BJMF parameters on the final constraints results. In the BJMF model used in this work, the magnetic field strength depends on the parameters B_0 , δ_D , n_0 , and r_{VHE} . Among these parameters, the value of the core magnetic field strength at r_{VHE} directly characterizes the magnetic field strength and could significantly affect the ALP-photon oscillation effect. In the above analysis, B_0 , δ_D , n_0 , and r_{VHE} are taken to be the benchmark values, which are derived from the fit to the experimental data using the synchrotron self-Compton model in other references. However, we have the conclusion in our previous work [52] that the final constraints are significantly affected by the magnetic field strength in the emission region B_0 and especially the distance of the emission region to the central black hole r_{VHE} . The constraints would become stringent for large B_0 and r_{VHE} , while the changes of the other parameters do not significantly affect the results.

VI. CONCLUSION

In this work, we reanalyze the ALP-photon oscillation effect in the spectra of the blazars Mrk 421 and PG 1553+113 measured by MAGIC and *Fermi*-LAT during the common operation time, which cover fifteen phases of Mrk 421 and five phases of PG 1553+113, respectively. We find that not all the observations of these phases can be individually used to set the 95% C.L. constraint on the ALP parameter space. However, the constraint can be significantly improved if the analyses for the observations of these phases are combined.

For Mrk 421, compared with the limits set by the PKS 2155–304 observation of H.E.S.S. [48] and the NGC 1275 observation of *Fermi*-LAT [49], we find that the combined γ -ray observations of MAGIC and *Fermi*-LAT with fifteen phases have excluded the ALP parameter region

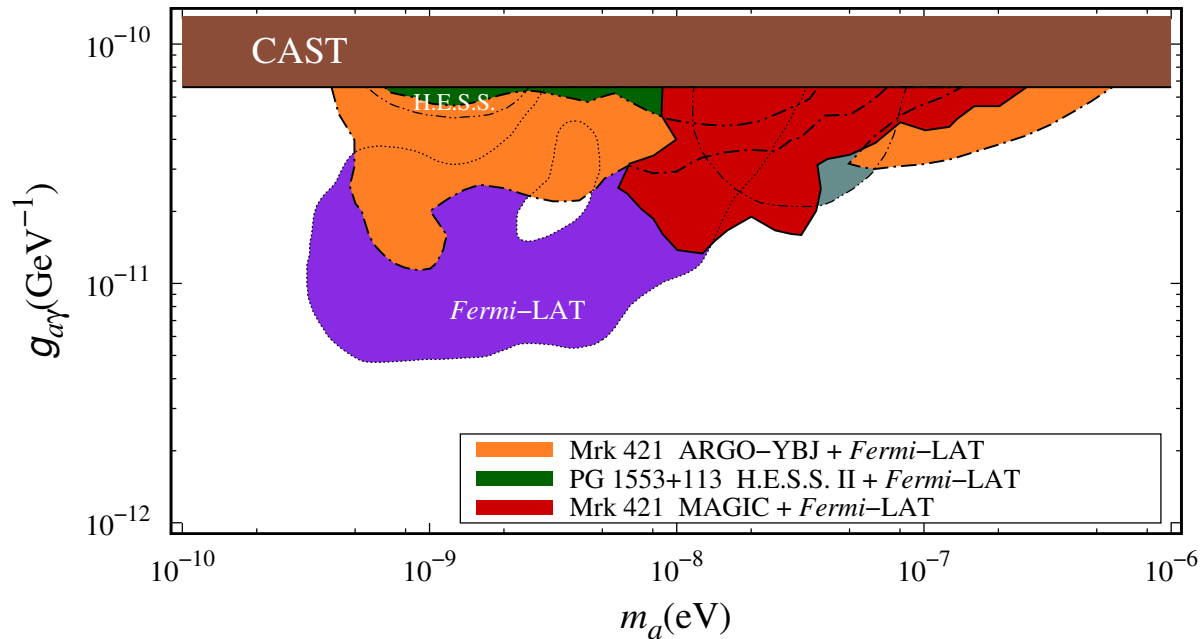


FIG. 4. The excluded regions at 95% C.L. in the $m_a - g_{a\gamma}$ plane set by the Mrk 421 observations of MAGIC and *Fermi*-LAT. The red contour represents the Mrk 421 combined constraint result derived with the MAGIC and *Fermi*-LAT data. For comparison, the constraints set by CAST [80], the PKS 2155–304 observation of H.E.S.S. [48], and the NGC 1275 observation of *Fermi*-LAT [49] are shown. We also show the constraints set by the Mrk 421 observations using the data from ARGO-YBJ and *Fermi*-LAT [52], and the PG 1553+113 observations using the data from H.E.S.S. II and *Fermi*-LAT [51]. The combined constraints set by the PG 1553+113 observations using the data from MAGIC and *Fermi*-LAT in this work (see Fig. 3) are not shown here.

with the ALP-photon coupling of $g_{a\gamma} \gtrsim 2 \times 10^{-11} \text{ GeV}^{-1}$ for the ALP mass of $\sim 8 \times 10^{-9} \text{ eV} \lesssim m_a \lesssim 2 \times 10^{-7} \text{ eV}$ at 95% C.L. However, we find that the ALP-photon oscillation would improve the fit to the observed spectra of PG 1553+113 with five phases and find some favored parameter regions at 95% C.L.

In the future, the new generation VHE γ -ray observations, such as Cherenkov Telescope Array (CTA) [81], Large High Altitude Air Shower Observatory (LHAASO) [82], High Energy cosmic-Radiation Detection (HERD) [83], Gamma-Astronomy Multifunction Modules Apparatus (GAMMA 400) [84], and Tunka Advanced Instrument for Gamma-ray and Cosmic ray Astrophysics-Hundred Square km Cosmic ORigin Explorer (TAIGA-HiSCORE) [85], will collect more data for the high energy γ -ray sources at large distances from the Earth with high

precision. Thus, using these VHE γ -ray observations results, it is possible to set the more stringent constraints on the ALP parameter space.

ACKNOWLEDGMENTS

The authors would like to thank Mireia Nievas Rosillo for providing the energy spectra of Mrk 421 and PG 1553+113 by MAGIC and *Fermi*-LAT in the common operation time. We also thank Jun-Guang Guo for providing helpful discussions and comments. This work is supported by the National Key R&D Program of China (Grant No. 2016YFA0400200) and the National Natural Science Foundation of China (Grants No. U1738209 and No. 11851303).

-
- [1] R. D. Peccei, *Lect. Notes Phys.* **741**, 3 (2008), arXiv:hep-ph/0607268.
 [2] J. E. Kim and G. Carosi, *Rev. Mod. Phys.* **82**, 557 (2010), arXiv:0807.3125 [hep-ph].
 [3] H.-Y. Cheng, *Phys. Rept.* **158**, 1 (1988).
 [4] G. Grilli di Cortona, E. Hardy, J. Pardo Vega, and G. Villadoro, *JHEP* **01**, 034 (2016), arXiv:1511.02867

- [hep-ph].
 [5] L. Di Luzio, M. Giannotti, E. Nardi, and L. Visinelli, *Phys. Rept.* **870**, 1 (2020), arXiv:2003.01100 [hep-ph].
 [6] R. Peccei and H. R. Quinn, *Phys. Rev. D* **16**, 1791 (1977).
 [7] R. Peccei and H. R. Quinn, *Phys. Rev. Lett.* **38**, 1440 (1977).
 [8] S. Weinberg, *Phys. Rev. Lett.* **40**, 223 (1978).

- [9] F. Wilczek, *Phys. Rev. Lett.* **40**, 279 (1978).
- [10] J. E. Kim, *Phys. Rept.* **150**, 1 (1987).
- [11] J. E. Kim, *Phys. Rev. Lett.* **43**, 103 (1979).
- [12] M. A. Shifman, A. I. Vainshtein, and V. I. Zakharov, *Nucl. Phys. B* **166**, 493 (1980).
- [13] M. Dine, W. Fischler, and M. Srednicki, *Phys. Lett. B* **104**, 199 (1981).
- [14] A. R. Zhitnitsky, *Sov. J. Nucl. Phys.* **31**, 260 (1980).
- [15] P. Svrcek and E. Witten, *JHEP* **06**, 051 (2006), [arXiv:hep-th/0605206](#).
- [16] A. Arvanitaki, S. Dimopoulos, S. Dubovsky, N. Kaloper, and J. March-Russell, *Phys. Rev. D* **81**, 123530 (2010), [arXiv:0905.4720 \[hep-th\]](#).
- [17] D. J. E. Marsh, *Phys. Rept.* **643**, 1 (2016), [arXiv:1510.07633 \[astro-ph.CO\]](#).
- [18] J. Preskill, M. B. Wise, and F. Wilczek, *Phys. Lett. B* **120**, 127 (1983).
- [19] L. Abbott and P. Sikivie, *Phys. Lett. B* **120**, 133 (1983).
- [20] M. Dine and W. Fischler, *Phys. Lett. B* **120**, 137 (1983).
- [21] M. Khlopov, A. Sakharov, and D. Sokoloff, *Nucl. Phys. B Proc. Suppl.* **72**, 105 (1999).
- [22] P. Sikivie, *Int. J. Mod. Phys. A* **25**, 554 (2010), [arXiv:0909.0949 \[hep-ph\]](#).
- [23] G. Raffelt and L. Stodolsky, *Phys. Rev. D* **37**, 1237 (1988).
- [24] A. De Angelis, M. Roncadelli, and O. Mansutti, *Phys. Rev. D* **76**, 121301 (2007), [arXiv:0707.4312 \[astro-ph\]](#).
- [25] D. Hooper and P. D. Serpico, *Phys. Rev. Lett.* **99**, 231102 (2007), [arXiv:0706.3203 \[hep-ph\]](#).
- [26] M. Simet, D. Hooper, and P. D. Serpico, *Phys. Rev. D* **77**, 063001 (2008), [arXiv:0712.2825 \[astro-ph\]](#).
- [27] A. Mirizzi and D. Montanino, *JCAP* **12**, 004 (2009), [arXiv:0911.0015 \[astro-ph.HE\]](#).
- [28] A. V. Belikov, L. Goodenough, and D. Hooper, *Phys. Rev. D* **83**, 063005 (2011), [arXiv:1007.4862 \[astro-ph.HE\]](#).
- [29] A. De Angelis, G. Galanti, and M. Roncadelli, *Phys. Rev. D* **84**, 105030 (2011), [Erratum: *Phys. Rev. D* **87**, 109903 (2013)], [arXiv:1106.1132 \[astro-ph.HE\]](#).
- [30] A. Dominguez, M. A. Sanchez-Conde, and F. Prada, *JCAP* **11**, 020 (2011), [arXiv:1106.1860 \[astro-ph.CO\]](#).
- [31] D. Horns, L. Maccione, M. Meyer, A. Mirizzi, D. Montanino, and M. Roncadelli, *Phys. Rev. D* **86**, 075024 (2012), [arXiv:1207.0776 \[astro-ph.HE\]](#).
- [32] O. Mena and S. Razzaque, *JCAP* **11**, 023 (2013), [arXiv:1306.5865 \[astro-ph.HE\]](#).
- [33] M. Meyer, D. Horns, and M. Raue, *Phys. Rev. D* **87**, 035027 (2013), [arXiv:1302.1208 \[astro-ph.HE\]](#).
- [34] R. Reesman and T. Walker, *JCAP* **08**, 021 (2014), [arXiv:1402.2533 \[astro-ph.HE\]](#).
- [35] M. Meyer, D. Montanino, and J. Conrad, *JCAP* **09**, 003 (2014), [arXiv:1406.5972 \[astro-ph.HE\]](#).
- [36] M. Meyer and J. Conrad, *JCAP* **12**, 016 (2014), [arXiv:1410.1556 \[astro-ph.HE\]](#).
- [37] M. Meyer, M. Giannotti, A. Mirizzi, J. Conrad, and M. Sánchez-Conde, *Phys. Rev. Lett.* **118**, 011103 (2017), [arXiv:1609.02350 \[astro-ph.HE\]](#).
- [38] B. Berenji, J. Gaskins, and M. Meyer, *Phys. Rev. D* **93**, 045019 (2016), [arXiv:1602.00091 \[astro-ph.HE\]](#).
- [39] J. Majumdar, F. Calore, and D. Horns, *PoS IFS2017*, 168 (2017), [arXiv:1711.08723 \[hep-ph\]](#).
- [40] K. Kohri and H. Kodama, *Phys. Rev. D* **96**, 051701 (2017), [arXiv:1704.05189 \[hep-ph\]](#).
- [41] G. Galanti and M. Roncadelli, *Phys. Rev. D* **98**, 043018 (2018), [arXiv:1804.09443 \[astro-ph.HE\]](#).
- [42] G. Galanti and M. Roncadelli, *JHEAp* **20**, 1 (2018), [arXiv:1805.12055 \[astro-ph.HE\]](#).
- [43] G. Galanti, F. Tavecchio, M. Roncadelli, and C. Evoli, *Mon. Not. Roy. Astron. Soc.* **487**, 123 (2019), [arXiv:1811.03548 \[astro-ph.HE\]](#).
- [44] C. Zhang, Y.-F. Liang, S. Li, N.-H. Liao, L. Feng, Q. Yuan, Y.-Z. Fan, and Z.-Z. Ren, *Phys. Rev. D* **97**, 063009 (2018), [arXiv:1802.08420 \[hep-ph\]](#).
- [45] Y.-F. Liang, C. Zhang, Z.-Q. Xia, L. Feng, Q. Yuan, and Y.-Z. Fan, *JCAP* **06**, 042 (2019), [arXiv:1804.07186 \[hep-ph\]](#).
- [46] G. Long, W. Lin, P. Tam, and W. Zhu, *Phys. Rev. D* **101**, 063004 (2020), [arXiv:1912.05309 \[astro-ph.HE\]](#).
- [47] M. Libanov and S. Troitsky, *Phys. Lett. B* **802**, 135252 (2020), [arXiv:1908.03084 \[astro-ph.HE\]](#).
- [48] A. Abramowski et al. (H.E.S.S.), *Phys. Rev. D* **88**, 102003 (2013), [arXiv:1311.3148 \[astro-ph.HE\]](#).
- [49] M. Ajello et al. (Fermi-LAT), *Phys. Rev. Lett.* **116**, 161101 (2016), [arXiv:1603.06978 \[astro-ph.HE\]](#).
- [50] X.-J. Bi, Y. Gao, J. Guo, N. Houston, T. Li, F. Xu, and X. Zhang, *Phys. Rev. D* **103**, 043018 (2021), [arXiv:2002.01796 \[astro-ph.HE\]](#).
- [51] J. Guo, H.-J. Li, X.-J. Bi, S.-J. Lin, and P.-F. Yin, *Chin. Phys. C* **45**, 025105 (2021), [arXiv:2002.07571 \[astro-ph.HE\]](#).
- [52] H.-J. Li, J.-G. Guo, X.-J. Bi, S.-J. Lin, and P.-F. Yin, *Phys. Rev. D* **103**, 083003 (2021), [arXiv:2008.09464 \[astro-ph.HE\]](#).
- [53] R. Buehler, G. Gallardo, G. Maier, A. Domínguez, M. López, and M. Meyer, *JCAP* **09**, 027 (2020), [arXiv:2004.09396 \[astro-ph.HE\]](#).
- [54] J.-G. Cheng, Y.-J. He, Y.-F. Liang, R.-J. Lu, and E.-W. Liang, *Phys. Lett. B* **821**, 136611 (2021), [arXiv:2010.12396 \[astro-ph.HE\]](#).
- [55] G. Long, S. Chen, S. Xu, and H.-H. Zhang, *Phys. Rev. D* **104**, 083014 (2021), [arXiv:2101.10270 \[astro-ph.HE\]](#).
- [56] J. Davies, M. Meyer, and G. Cotter, *Phys. Rev. D* **103**, 023008 (2021), [arXiv:2011.08123 \[astro-ph.HE\]](#).
- [57] Y.-F. Liang, X.-F. Zhang, J.-G. Cheng, H.-D. Zeng, Y.-Z. Fan, and E.-W. Liang, (2020), [arXiv:2012.15513 \[astro-ph.HE\]](#).
- [58] J. Zhou, Z. Wang, F. Huang, and L. Chen, *JCAP* **08**, 007 (2021), [arXiv:2102.05833 \[astro-ph.HE\]](#).
- [59] I. Batković, A. De Angelis, M. Doro, and M. Manganaro, *Universe* **7**, 185 (2021), [arXiv:2106.03424 \[astro-ph.HE\]](#).
- [60] H. Abdalla et al. (H.E.S.S., LAT), *Astron. Astrophys.* **600**, A89 (2017), [arXiv:1612.01843 \[astro-ph.HE\]](#).
- [61] B. Bartoli et al. (ARGO-YBJ), *Astrophys. J. Suppl.* **222**, 6 (2016), [arXiv:1511.06851 \[astro-ph.HE\]](#).
- [62] V. Acciari et al. (MAGIC), *Mon. Not. Roy. Astron. Soc.* **486**, 4233 (2019), [arXiv:1904.00134 \[astro-ph.HE\]](#).
- [63] F. Tavecchio, M. Roncadelli, and G. Galanti, *Phys. Lett. B* **744**, 375 (2015), [arXiv:1406.2303 \[astro-ph.HE\]](#).
- [64] M. C. Begelman, R. D. Blandford, and M. J. Rees, *Rev. Mod. Phys.* **56**, 255 (1984).
- [65] G. Ghisellini and F. Tavecchio, *Mon. Not. Roy. Astron. Soc.* **397**, 985 (2009), [arXiv:0902.0793 \[astro-ph.CO\]](#).
- [66] R. Pudritz, M. Hardcastle, and D. Gabuzda, *Space Sci. Rev.* **169**, 27 (2012), [arXiv:1205.2073 \[astro-ph.HE\]](#).
- [67] S. P. O'Sullivan and D. C. Gabuzda, *Mon. Not. Roy. Astron. Soc.* **400**, 26 (2009), [arXiv:0907.5211 \[astro-ph.CO\]](#).

- [68] A. Celotti and G. Ghisellini, *Mon. Not. Roy. Astron. Soc.* **385**, 283 (2008), arXiv:0711.4112 [astro-ph].
- [69] F. Tavecchio, M. Roncadelli, G. Galanti, and G. Bonnoli, *Phys. Rev. D* **86**, 085036 (2012), arXiv:1202.6529 [astro-ph.HE].
- [70] C. Carilli and G. Taylor, *Ann. Rev. Astron. Astrophys.* **40**, 319 (2002), arXiv:astro-ph/0110655.
- [71] F. Govoni and L. Feretti, *Int. J. Mod. Phys. D* **13**, 1549 (2004), arXiv:astro-ph/0410182.
- [72] K. Subramanian, A. Shukurov, and N. E. L. Haugen, *Mon. Not. Roy. Astron. Soc.* **366**, 1437 (2006), arXiv:astro-ph/0505144.
- [73] M. Pshirkov, P. Tinyakov, and F. Urban, *Phys. Rev. Lett.* **116**, 191302 (2016), arXiv:1504.06546 [astro-ph.CO].
- [74] P. Ade et al. (Planck), *Astron. Astrophys.* **594**, A19 (2016), arXiv:1502.01594 [astro-ph.CO].
- [75] A. Franceschini, G. Rodighiero, and M. Vaccari, *Astron. Astrophys.* **487**, 837 (2008), arXiv:0805.1841 [astro-ph].
- [76] R. Jansson and G. R. Farrar, *Astrophys. J. Lett.* **761**, L11 (2012), arXiv:1210.7820 [astro-ph.GA].
- [77] J. Aleksić et al., *Astropart. Phys.* **72**, 61 (2016), arXiv:1409.6073 [astro-ph.IM].
- [78] J. Aleksić et al. (MAGIC), *Astropart. Phys.* **72**, 76 (2016), arXiv:1409.5594 [astro-ph.IM].
- [79] W. Atwood et al. (Fermi-LAT), *Astrophys. J.* **697**, 1071 (2009), arXiv:0902.1089 [astro-ph.IM].
- [80] V. Anastassopoulos et al. (CAST), *Nature Phys.* **13**, 584 (2017), arXiv:1705.02290 [hep-ex].
- [81] B. Acharya et al. (CTA Consortium), *Astropart. Phys.* **43**, 3 (2013).
- [82] Z. Cao (LHAASO), *Chin. Phys. C* **34**, 249 (2010).
- [83] X. Huang et al., *Astropart. Phys.* **78**, 35 (2016), arXiv:1509.02672 [astro-ph.HE].
- [84] A. M. Galper et al., *Adv. Space Res.* **51**, 297 (2013), arXiv:1201.2490 [astro-ph.IM].
- [85] L. A. Kuzmichev et al., *Phys. Atom. Nucl.* **81**, 497 (2018).

TABLE I. List of the best-fit values of the χ^2 without/with ALP for Mrk 421 with fifteen phases and PG 1553+113 with five phases, respectively. Period stands for the corresponding MAGIC observation. The intrinsic blazar energy spectra models are shown. The effective d.o.f. of the TS distributions and the values of $\Delta\chi^2$ corresponding to 95% C.L. are also listed. The combined results for these phases are also shown.

Source [period]	Tstart	Tstop	Model	$\chi^2_{w/oALP}$	χ^2_{min}	Effective d.o.f.	$\Delta\chi^2$
Mrk 421 [20130410]	2013-04-09T12:00	2013-04-10T12:00	SEPWL	12.244	8.845	4.45	10.232
Mrk 421 [20130411]	2013-04-10T18:00	2013-04-11T06:00	ELP	16.213	10.124	6.85	13.868
Mrk 421 [20130412]	2013-04-11T18:00	2013-04-12T06:00	ELP	8.911	6.186	7.54	14.868
Mrk 421 [20130413a]	2013-04-12T12:00	2013-04-13T12:00	ELP	16.007	12.928	8.00	15.527
Mrk 421 [20130413b]	2013-04-12T12:00	2013-04-13T12:00	SEPWL	9.733	8.645	4.72	10.657
Mrk 421 [20130413c]	2013-04-12T12:00	2013-04-13T12:00	SEPWL	10.049	7.537	4.56	10.406
Mrk 421 [20130414]	2013-04-13T12:00	2013-04-14T12:00	ELP	22.391	13.749	9.22	17.245
Mrk 421 [20130415a]	2013-04-14T21:17	2013-04-15T04:13	ELP	5.774	4.777	5.23	11.447
Mrk 421 [20130415b]	2013-04-14T21:17	2013-04-15T04:13	SEPWL	13.426	10.016	5.02	11.124
Mrk 421 [20130415c]	2013-04-14T21:17	2013-04-15T04:13	SEPWL	5.056	4.012	4.71	10.641
Mrk 421 [20130416]	2013-04-15T12:00	2013-04-16T09:00	SEPWL	32.863	19.552	5.48	11.829
Mrk 421 [20130417]	2013-04-16T18:00	2013-04-17T06:00	SEPWL	26.050	11.174	4.99	11.077
Mrk 421 [20130418]	2013-04-17T12:00	2013-04-18T12:00	EPWL	13.345	9.038	5.56	11.950
Mrk 421 [20130419]	2013-04-18T12:00	2013-04-19T12:00	ELP	3.609	1.964	4.07	9.625
Mrk 421 [20140426]	2014-04-25T18:00	2014-04-26T06:00	ELP	25.809	15.184	6.19	12.896
PG 1553+113 [ST0202]	2012-02-28T12:00	2012-03-04T12:00	EPWL	2.326	0.895	3.31	8.371
PG 1553+113 [ST0203]	2012-03-13T12:00	2012-05-02T12:00	SEPWL	15.566	5.547	5.93	12.508
PG 1553+113 [ST0302]	2013-04-07T12:00	2013-06-12T12:00	SEPWL	5.407	1.618	4.07	9.625
PG 1553+113 [ST0303]	2014-03-11T12:00	2014-03-25T12:00	EPWL	10.167	6.031	6.68	13.620
PG 1553+113 [ST0306]	2015-01-25T12:00	2015-08-07T12:00	SEPWL	4.679	1.001	3.52	8.723
Combined Mrk 421				221.480	204.554	31.17	45.206
Combined PG 1553+113				38.144	19.984	8.61	16.390